Development of Morphological Diversity of Dendrites in *Drosophila* by the BTB-Zinc Finger Protein Abrupt

Kaoru Sugimura,[1,2] Daisuke Satoh,[1,2]
Patricia Estes,[3,5] Stephen Crews,[3]
and Tadashi Uemura[1,4,6,*]
[1]Laboratory of Molecular Genetics
The Institute for Virus Research
[2]Graduate School of Science
Kyoto University
Kyoto 606-8507
Japan
[3]Biochemistry and Biophysics
School of Medicine
The University of North Carolina at Chapel Hill
Chapel Hill, North Carolina 27599
[4]Core Research for Evolutional Science
   and Technology (CREST)
Japan Science and Technology
Kawaguchi, Saitama 332-0012
Japan

Summary

Morphological diversity of dendrites contributes to specialized functions of individual neurons. In the present study, we examined the molecular basis that generates distinct morphological classes of *Drosophila* dendritic arborization (da) neurons. da neurons are classified into classes I to IV in order of increasing territory size and/or branching complexity. We found that Abrupt (Ab), a BTB-zinc finger protein, is expressed selectively in class I cells. Misexpression of *ab* in neurons of other classes directed them to take the appearance of cells with smaller and/or less elaborated arbors. Loss of *ab* functions in class I neurons resulted in malformation of their typical comb-like arbor patterns and generation of supernumerary branch terminals. Together with the results of monitoring dendritic dynamics of *ab*-misexpressing cells or *ab* mutant ones, all of the data suggested that Ab endows characteristics of dendritic morphogenesis of the class I neurons.

Introduction

Morphologies of dendritic trees are highly variable from one neuronal type to another, and this diversity contributes to differential processing and computation of synaptic or sensory inputs (Scott and Luo, 2001; Masland, 2001; Whitford et al., 2002; Häusser and Mel, 2003; Wong and Ghosh, 2002; Jan and Jan, 2003; Grueber and Jan, 2004). For example, dendritic geometry plays key roles in shaping intrinsic firing patterns, both back and forward propagation of action potentials and dendritic

spikes, and coincidence detection (Mainen and Sejnowski, 1996; Vetter et al., 2001; Schaefer et al., 2003). Therefore, the proper function of the nervous system relies not only on correct targeting of axons or dendrites, but also on development of class-specific dendritic patterns. However, genetic programs underlying dendritic diversity are not yet well understood.

Dendritic arborization (da) neurons in the *Drosophila* peripheral nervous system (PNS) provide an excellent model system to tackle this question in vivo. The embryonic PNS organizes a stereotyped pattern of identified sensory neurons, and da neurons constitute a subfamily of multidendritic (md) neurons (Figure 1A; Bodmer and Jan, 1987; Jan and Jan, 1993; Campos-Ortega and Hartenstein, 1997). da neurons grow two-dimensional dendrites underneath the epidermis during late embryonic, larval, and pupal stages (Bodmer and Jan, 1987; Williams and Truman, 2004). On the basis of images of single da neurons in mature larva, the 15 da neurons in each abdominal hemisegment are classified into four categories, classes I–IV, in order of increasing territory size and/or arbor complexity (Figure 1A; Grueber et al., 2002). Class I neurons are characterized by formation of simple comb-like small dendritic trees (Figure 1B), whereas class IV develop far more complicated and expansive arbors (Figure 1C; Grueber et al., 2002; Sugimura et al., 2003).

Class-specific transgenic GFP markers have made it feasible to undertake time-lapse analysis of da neurons from dendritic birth till maturation, and such analyses have provided us insight into the cellular basis of class-specific dendritic morphogenesis (Grueber et al., 2003b; Sugimura et al., 2003). Class I neurons and class IV neurons employ distinct strategies of dendritic emergence from the cell body and branching, which contribute to differences in their basic arbor patterns. In contrast to class I neurons, class IV neurons continue to elaborate higher-order branches throughout larval stages. In addition to these distinct developmental dynamics, class IV cells are characterized by their class-specific mutual avoidance of both isoneuronal and heteroneuronal dendritic branches, and this allows complete but minimal overlapping innervation of the body wall (described later in Figure 4; Sugimura et al., 2003; Grueber et al., 2003b). On the other hand, class I and class II neurons do not show such inhibitory dendrodendritic interaction to shape the territorial boundary between the same class of neurons, and dendritic branches of class III neurons avoid each other only at their short terminal extensions (Grueber et al., 2003b).

Then what are molecular mechanisms that make dendritic behaviors of each class distinct? Our previous enhancer trap screening aimed at hunting for either pan-da or subset markers and then looking for trapped genes that might be expressed in a particular class(es), with the expectation of roles of those genes in class-specific dendrite morphogeneis (Sugimura et al., 2003). Here we report that one of our class I markers trapped *abrupt* (*ab*) and that the Ab protein was selectively expressed in class I da neurons. The expression profile of Ab was

*Correspondence: tuemura@virus.kyoto-u.ac.jp
[5]Present address: Department of Genetics, North Carolina State University, North Carolina 27695.
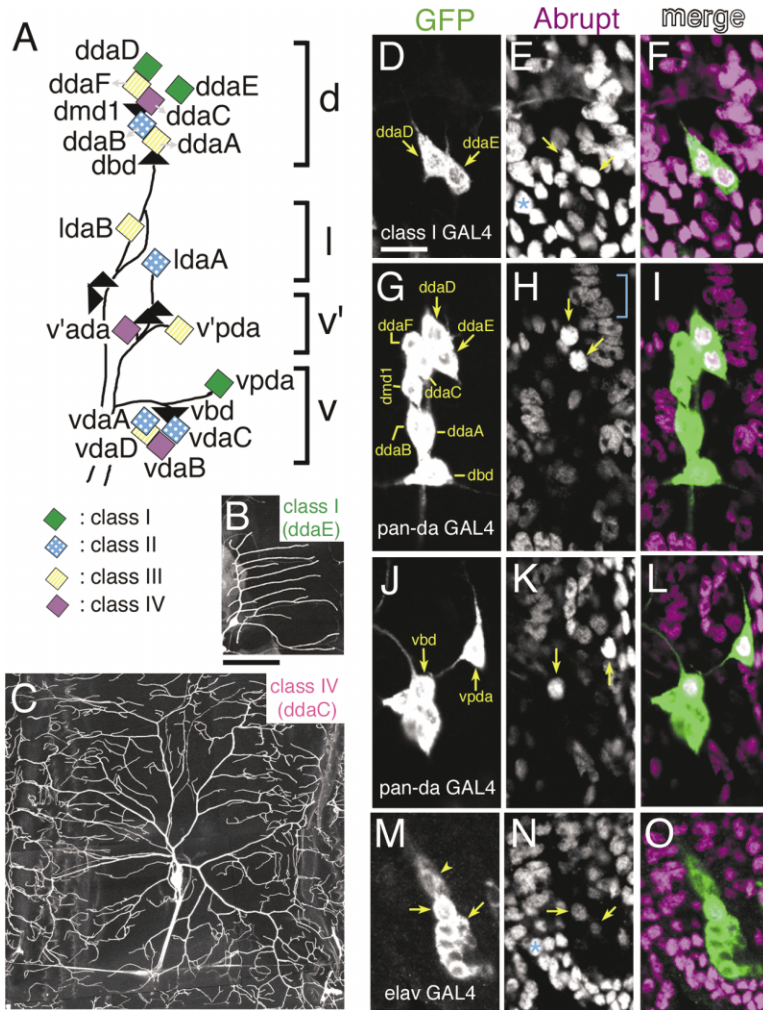[6]Present address: Graduate School of Biostudies, Kyoto University, Kyoto 606-8502, Japan.

Figure 1. Distinct Morphological Classes of da Neurons and Selective *ab* Expression in Class I

(A) A diagram of positions of multidendritic (md) neurons in an abdominal hemisegment of the *Drosophila* embryonic and larval PNS. Diamonds represent individual dendritic arborization (da) neurons and triangles represent other types of md neurons. Besides all da neurons, only two bipolar dendrite neurons (dbd and vbd) and dmd1 that appear in subsequent figures are indicated for simplicity. d, l, v′, and v represent dorsal, lateral, ventral prime, and ventral clusters, respectively. Each class of the da neurons is differently colored. Black lines represent fascicles of axons that extend from the neuronal cell bodies. In this and all subsequent figures, anterior is to the left and dorsal is at the top.

(B and C) Morphologies of a class I neuron (ddaE) and the class IV neuron (ddaC) in the dorsal cluster at 74–78 hr after egg laying (AEL). Genotypes were *IG1-1/mCD8::GFP* (B) and *NP7028 mCD8::GFP/mCD8::GFP* (C).

(D–O) Expression patterns of Abrupt (Ab) protein in dorsal (D–I and M–O) and ventral (J–L) clusters.

(D–L) Stage 16 embryo of a class I marker line (D–F, *NP2225/mCD8::GFP*) or that of a pan-da marker line (G–L, *IG1-2 mCD8::GFP*) was doubly labeled for GFP (D, G, J, and green in F, I, and L) and for Ab (E, H, K, and magenta in F, I, and L). Merged images shown in (F), (I), and (L). Among da neurons, Ab was expressed highly and in a selectable manner in all of the three class I neurons, ddaD and ddaE (arrows in D, E, G, and H) and vpda (right arrow in J and K). The Ab expression level was also high in vbd (left arrow in J and K). We did not detect significant signals in other neurons in the abdominal segment. Outside the nervous system, Ab was produced by epidermal cells (asterisks in E and N) and muscles (bracket in H).

(M–O) Stage 13 embryo of a panneuronal marker line, *elav-GAL4 mCD8::GFP,* was stained for GFP (M and green in O) and Ab (N and magenta in O). Two neurons in the dorsal cluster were weakly stained at this stage, whereas other neurons including those indicated by the arrowhead in (M) (possibly one of external sensory neurons) were not.

Scale bars equal 50 μm for (B) and (C) and 10 μm for (D)–(O).

roughly complementary to that of Cut, a homeodomain protein. The level of Cut is below the limit of detection in class I neurons, whereas it is either moderate or strong in class II to IV neurons. Most importantly, those different levels of Cut regulate dendrite growth as well as class-specific terminal branching (Grueber et al., 2003a).

We addressed whether Ab might be required for class I dendrite morphogenesis or not and whether the *ab* gene must be silent in class II-IV cells for their normal dendrite development. Loss of *ab* function in class I neurons caused deformation of the characteristic comb-like shape of their dendritic arbors, produced excess branch terminals of all of three cells examined, and increased in the territory size of one cell. Misexpression of *ab* influenced dendritic designs of neurons of class II to IV, which do not express *ab* normally; that is, *ab*-misexpressing neurons of class II to IV generated less expansive dendritic trees, and those of class III and IV had fewer branch terminals compared with control cells. These data showed that Ab directed morphologically

simple and small dendrites with a comb-like shape, which are characteristic of class I da neurons. We further addressed whether or not *ab* and *cut* influenced each other at the level of gene expression and at the level of dendritic morphology as a final read-out.

Results

Selective Expression of *abrupt*
in Class I da Neurons
One of our class I marker lines is *NP2225*, which labels all of the three class I da neurons, but no other da neurons, in the abdominal hemisegment (Figures 1D and 1F; Sugimura et al., 2003). In the genome of *NP2225*, a P element was inserted into the first intron of the *abrupt* (*ab*) gene (see details in Experimental Procedures). *ab* encodes a BTB domain-zinc finger protein and is required for neuromuscular connectivity in the embryo (Hu et al., 1995). By using an antibody to Ab protein, we detected immunoreactivity in the nuclei of the three

class I da neurons, but expression in the other classes of da neurons was below the limit of our detection (Figures 1D–1O). Outside the nervous system, Ab was expressed in epidermal cells and muscles (see asterisks in Figures 1E and 1N and bracket in Figure 1H, respectively; Hu et al., 1995). Immunoreactivity per nucleus was comparable between the class I da neurons and epidermal cells, and muscle nuclei were stained less brightly around 13 hr after egg laying (AEL) (stage 16), when dendritogenesis was initiated (Figures 1E, 1H, and 1K). The selective expression within the da neuron classes persisted at third instar larval stages (data not shown). At earlier stages such as 9–10 hr AEL (stage 13) when all da neurons are born, a small subset of peripheral neurons was stained, but very faintly compared with epidermal cells (Figures 1M–1O), and those positive neurons were possibly class I neurons.

Ectopic Expression of *ab* Reduced the Size of Overall Dendritic Trees

To address whether the class I-selective expression of *ab* plays roles in class-specific dendrite patterning or not, we took two complementary approaches: one was to study effects of misexpression of *ab* on morphogenesis of class II–IV neuron dendrites, which innervate larger regions of the body wall than class I dendrites. The other was to observe dendritic arbors of class I neurons, which express *ab* normally, in *ab* loss-of-function mutant cells. We first present the results of our misexpression experiments (Figures 2–5).

We drove *ab* expression in all da neurons in a postmitotic manner by using pan-da GAL4 lines, and this pan-da expression caused dramatic alteration of overall patterns of dendritic arbors (Figures 2A–2D). The body wall of the control larva is entirely covered with dendritic trees of da neurons from 30–35 hr AEL onward (Figures 2A and 2C; Gao et al., 2000; Grueber et al., 2003b; Sugimura et al., 2003). Although the larvae that expressed *ab* in the pan-da fashion kept expanding their body walls till late second instar larval stages, large dendrite-free zones appeared around segmental boundaries and dorsal midlines, which lie midway between ipsilateral and contralateral dorsal clusters (Figures 2B and 2D). In normal development, those zones are covered by dendritic branches of class II–IV neurons that form larger dendritic fields than class I cells; and class IV branches contribute most to this filling (Grueber et al., 2002). We imaged cell bodies of the GFP-labeled neurons and confirmed that *ab* ectopic expression did not alter the total number or the stereotypic arrangement of da neurons in each cluster (Figures 2E and 2F). These results suggest the possibility that *ab* expression reduced the size of dendritic trees of class II–IV.

This apparent downsizing effect occurred with complete penetrance (n > 150 dorsal clusters examined), irrespective of the expression of either of the two slightly distinct forms of Ab protein (Supplemental Figure S1 at http://www.neuron.org/cgi/content/full/43/6/809/DC1), and in clusters other than the dorsal one as well (yellow arrow in Figure 5B). Ab consists of a BTB domain and zinc fingers, and the expression of a truncated form that had only one of the two motifs did not result in morphologically visible effects (Supplemental Figure

S1). In our subsequent analysis, we focused mostly on the dorsal cluster in abdominal segments 2–6; this was partly because the dorsal cluster has all classes of da neurons and partly because axons extending from dorsally located neurons sometimes make images of the ventral, ventral-prime, and lateral clusters difficult to interpret (Figure 1A).

Dendritic Arbors of Class IV Neurons Became Downsized and Less Elaborated by *ab* Expression

To visualize how *ab* expression affected dendritic morphologies of individual classes, we performed single-cell analysis first on ddaC (class IV), which should have formed the most expansive and the most highly branched arbor in the dorsal cluster (Figure 1C). To extract pattern information about ddaC, we ablated all dorsal da neurons except for ddaC at embryonic or early larval stages and then tracked dendritic development of the remaining ddaC at subsequent stages.

When compared with the control ddaC, *ab*-misexpressing ddaC (*ab*+ddaC) at the same age showed a reduced size of its dendritic field and exhibited a visibly less complex morphology (compare Figures 3A with 3C; 3B with 3D; and 3E with 3F). Branch terminals of *ab*+ddaC did not reach far enough to meet those of adjacent cells. Furthermore, *ab*+ddaC did not elaborate higher-order fine branches in contrast to the wild-type cell (see arrow and bracket in Figures 3A and 3B). These phenotypes of the downsizing and the decrease in the terminal number were consolidated by our semiquantitative analysis (p < 0.01, Wilcoxon two-sample test; Figure 3G). When normalized to total dendritic length, the branching index (a measure of the number of branch terminals per dendritic length) of *ab*+ddaC was smaller than that of the control ddaC, and this decrease was statistically significant (p < 0.01, Wilcoxon two-sample test). This result supported that *ab* misexpression in ddaC made its dendritic arbor less complicated. In addition to the above single-cell analysis with the help of ablation, we used a GAL4 line that drove expression of both *ab* and GFP preferentially in class IV neurons and obtained qualitatively similar results (Figure 3H).

Dendritic Dynamics of *ab*-Expressing Class IV Neurons Resembled Those of Class I

It has been shown that the wild-type ddaC (class IV) continues branch formation throughout larval development (brackets and arrowheads of Figures 3A and 3B; n = 12; Sugimura et al., 2003); however, our time-lapse analysis showed that the *ab*+ddaC almost halted branching and stabilized its overall dendritic shape by midlarval stages (compare Figure 3C with 3D; n = 11). This temporal mode of *ab*+ddaC resembled what has been shown for class I neurons during normal development (Sugimura et al., 2003). In contrast to the arrest of higher-order branch formation, *ab* expression did not retard elongation of preexisting branches per se. This was shown by the fact that dendrites of *ab*+ddaC kept growing in a coordinated fashion with expansion of the body wall (compare scale bar of Figure 3C with that of 3D).

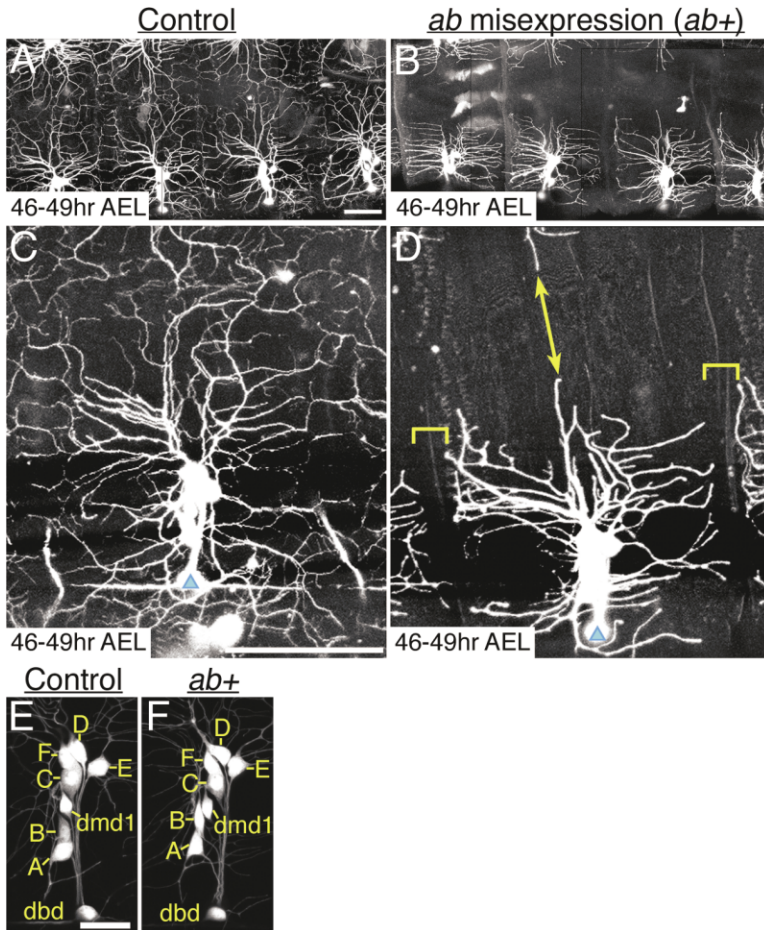In addition to their continuous branching, class IV

Figure 2. *ab* Misexpression Reduced the Size of Overall Dendritic Trees

Images of dorsal clusters at 46–49 hr AEL of control larvae (A, C, and E) and larvae that expressed *ab* at a high level and in all da neurons (B, D, and F). In larvae that misexpressed *ab*, large dendrite-free zones appeared between ipsilateral and contralateral clusters of da neurons (brackets and arrow, respectively, in D). Blue triangle represents dorsal bipolar dendrite neuron (dbd) in this and all subsequent figures. Close-up images of cell bodies at 46–49 hr AEL shown in (E) and (F). Individual da neurons were identified on the basis of the stereotypic spatial arrangement and the shape of cell bodies. ddaD (class I) is located most dorsally, and ddaE (class I) is at the most posterior position in the cluster. dbd is at the most ventral pole. At a position dorsal to dbd, there is a pair of ddaA (class III) and ddaB (class II); oval-shaped ddaB is dorsal to ddaA. ddaF (class III) is ventral to ddaD and attached to ddaC (class IV), which is bigger than ddaF. See also the diagram of Figure 1A. Genotypes of the control and *ab*-expressing larvae were *IG1-2 109(2)80 GFP[S65T]/+* and *IG1-2 109(2)80 GFP[S65T]/+; UAS-ab-L/+*, respectively. Scale bars equal 50 μm for (A)–(D) and 20 μm for (E) and (F).

dendrites are also characterized by their mutual avoidance of dendritic terminals, probably due to contact-meditated inhibition (Sugimura et al., 2003; Grueber et al., 2003b). This inhibition is manifested by robust "filling-in" response to microsurgeries, such as severing branches (Figures 4A and 4B; Sugimura et al., 2003). When roots of class IV neurons are destroyed in the wild-type animal, lateral branches spring from neighboring dendrites of the same cells and fill in open regions of the body wall (blue arrowheads in Figures 4A and 4B; n = 9). Furthermore, class IV cells in adjacent segments extend branches toward those regions (purple arrowheads in Figure 4B). When branches of *ab*+ddaC cells were severed, their remaining branches continued elongating as the body grew; however, they hardly sprouted toward the regions that would have been covered by the detached branches (blue arrowheads in Figures 4C and 4D; n = 13). Branches of neighboring segments hardly responded, either; consequently, the regions remained voided (box in Figure 4D). This poor filling-in reaction is also exactly what was shown for class I neurons (Sugimura et al., 2003; Grueber et al., 2003b).

Class III Dendrites Lost Protrusions or "Spikes" and Showed Reduced Field Size upon *ab* Misexpression
We also carried out single-cell analysis of the effects of *ab* misexpression on the morphogenesis of the other

three classes (Figure 5). Among the four classes of da neurons, dendritic arbors of class III neurons display a unique morphological feature, that is, many short and straight protrusions, designated "spikes" (brackets in Figure 5A; Grueber et al., 2002). One of the two dorsal class III neurons is ddaA, and we found that *ab*-misexpressing ddaA almost totally lost its spikes, which contributed to the substantial reduction in the number of branch terminals (Figure 5B). The terminal number of *ab*+ddaA was 26.0 ± 4.2 (n = 19), in contrast to the value for the control cell (>80, n = 23; see also Figure 10C). We also showed that *ab* expression led to a significant decrease in the field size (Figure 5C). Therefore, the results on ddaA (class III), together with those on ddaC (class IV), strongly suggest that *ab* misexpression directed both class III and IV neurons to take the appearance of less expansive dendritic arbors with fewer terminals.

ab Expression Decreased the Size, but Not the Terminal Number, of Class II Dendritic Trees
In normal development, class II neurons develop larger dendritic fields than those of class I, but branching complexities of these two classes are not significantly different (Grueber et al., 2002). *ab* misexpression reduced the field size of ddaB (class II), and this was quantified in a way that was applied to class III and IV neurons, that
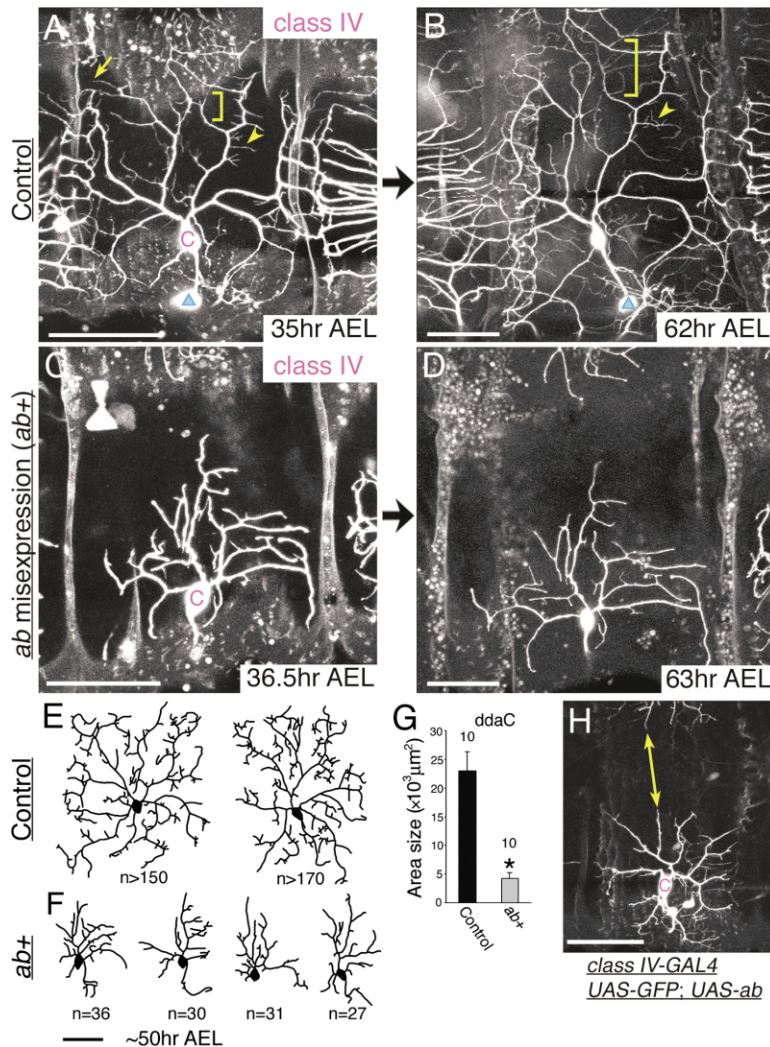
Figure 3. Decreases in the Field Size and the Terminal Number of Class IV ddaC Dendritic Trees by *ab* Misexpression

Single-cell analysis of the class IV neuron, ddaC, by cell ablation (A–G) or by preferential labeling of ddaC (H).

(A–D) Time-lapse recordings of the control ddaC (A and B) and the ddaC that misexpressed *ab* (C and D). In the middle hemisegment in each panel, all the dorsal da neurons except for ddaC had been ablated at 16–18 hr AEL and the remaining ddaCs were imaged at subsequent larval stages as indicated. Control ddaC continued to elaborate higher-order branches throughout larval development (brackets and arrowheads in [A] and [B]).

(E–G) All the dorsal da neurons, except for ddaC, were ablated at 24–26 hr AEL, and the remaining ddaC cells were imaged at around 50 hr AEL.

(E and F) Representative tracings of major dendritic branches of control ddaC (E) and all branches of *ab*-misexpressing ddaC (F). n represents the number of branch terminals, and the average value of *ab*-misexpressing ddaC was 30.4 ± 3.8.

(G) Quantification of dendritic field area for the control ddaC and the *ab*-misexpressing ddaC. Numbers of ddaC analyzed are indicated above each bar. Asterisk indicates $p < 0.01$ (Wilcoxon two-sample test). Genotypes were as described in the legend of Figure 2.

(H) Image of *ab*-misexpressing ddaC at 31.5–34 hr AEL. Genotype was *NP1161 GFP[S65T]/NP1161*; *UAS-ab-L/+*. Besides ddaC, ddaE was weakly labeled in this hemisegment. Arrow denotes large dendritic free zones between contralateral homologs.

Scale bars equal 50 μm for all panels.

is, by delineating a polygon connecting dendritic tips (Figures 5D–5G). However, values of standard deviations for control ddaB neurons were large, probably because ddaB formed more sparsely branched dendritic trees than class III and IV cells. As an alternative index for the size of ddaB, we measured the distance from the most distal tip of each dorsal-directed branch to the center of the cell body and confirmed the downsizing of *ab*+ddaB dendritic fields (Figure 5H).

The number of branch terminals of ddaB, in contrast to the field size, did not seem to decrease by the misexpression (compare Figure 5D with 5E and 5F). To assess this visible effect statistically, we needed to pinpoint dendritic branch tips. Anterior-directed branches of the control ddaB often overlapped with dendritic branches from the anterior adjacent segment, which obscured branch tips of the ddaB (see blue arrow in Figure 5D). To overcome this problem, we adopted two methods. First, we ablated almost all dorsal da neurons of two neighboring segments, except for two ddaBs, and then counted the terminal number of branches of the posterior ddaB (Figure 5I). Second, we excluded anteriorly oriented branches and counted the terminal number of

the rest (Figure 5J). Neither experiment indicated that *ab* misexpression affected the number of branches of ddaB in a statistically significant manner. Therefore, *ab* misexpression reduced the size of dendritic trees, but not the number of branch terminals, of class II cells. It should also be noted that the misexpression reduced the size values of all of ddaB (class II), ddaA (class III), and ddaC (class IV) to values comparable to those of class I cells (compare each of Figures 3G, 5C, and 5G with 5K) and that the terminal numbers of ddaA (class III) and ddaC (class IV) were similarly decreased (compare the values in Figure 3F with those in 5L). These results argue against the possibility that Ab exerted an inhibitory effect on dendritic branching in general; instead, they would support the hypothesis that *ab* misexpression transformed dendrite morphogenesis of class II-IV toward that of class I. The critical role of Ab in shaping class I dendrites was strengthened by loss-of-function analysis, as described below.

Class I da neurons expressed *ab* endogenously, and additional expression from the transgene did not alter their dendritic morphology. This result was obtained by using ablation protocol (Figures 5K and 5L) and by using
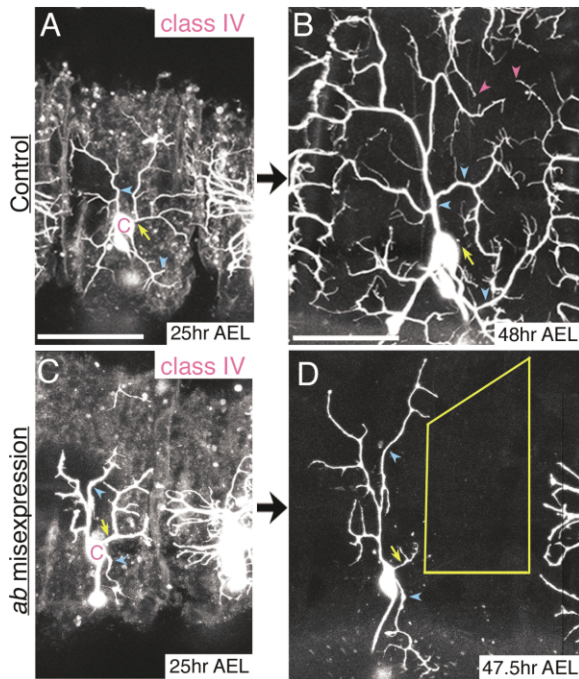
Figure 4. Poor Response of the *ab*-Misexpressing Class IV Neuron ddaC to the Loss of Isoneuronal or Heteroneuronal Branches

Time-lapse analysis of ddaC in response to severing of branches. Dendrite shafts of control ddaC (A and B) and *ab*-misexpressing ddaC (C and D) were destroyed at 25 hr AEL (yellow arrows in [A] and [C]) and observed one day later (B and D).

(A and B) Other isoneuronal branches of the control ddaC and heteroneuronal branches of adjacent ddaC filled in the voided field extensively (blue arrowhead and magenta arrowheads, respectively).

(C and D) Neither remaining isoneuronal branches (blue arrowheads) nor heteroneuronal branches of the *ab*-misexpressing ddaC filled in the voided field (box in [D]) that would have been covered by the severed branches. Genotypes were as described in the legend of Figure 2.

Scale bars equal 50 μm.

a GAL4 driver *NP2225* specific to class I neurons (data not shown).

In *ab* Loss-of-Function Mutants, Class I da Neurons Lost Their Characteristic Comb-like Arbor Patterns and Produced Supernumerary Dendritic Branches

The class I-selective expression of *ab* and the results of the misexpression studies led us to speculate that Ab might play some important roles in dendritic morphogenesis of class I neurons (ddaD, ddaE, and vpda) that normally express *ab*. We pursued this possibility by visualizing morphologies of class I neurons that were mutants for the *ab* locus. We employed two strong alleles: one was *ab*^clu1^, which is a nonsense mutation terminating the polypeptide between the BTB domain and zinc fingers (Hu et al., 1995; Supplemental Figure S1 at http:// www.neuron.org/cgi/content/full/43/6/809/DC1), and the other was *ab*^k02807^, a P insertion allele (Johannes and Preiss, 2002), which reduces Ab expression to the threshold level of our detection by immunostaining (data not shown). Animals of *ab*^clu1^ homozygotes or *ab*^clu1^/ *ab*^k02807^ transheterozygotes hatched and grew normally

till around 30 hr AEL. We used a GAL4 driver that highlights ddaE and vpda (Sugimura et al., 2003) and visualized its dendritic patterns in the wild-type and in the mutants. In each of over 300 mutant hemisegments examined, we could identify a single ddaE, strongly suggesting that the *ab* mutations did not affect generation of ddaE or reduce its viability.

In the wild-type at 24–26 hr AEL (about 2–6 hr after hatching), each ddaE neuron had generated two or three primary branches and one of them extended dorsally, from which secondary branches sprout and tended to elongate posteriorly in parallel (Figures 1B, 6A, and 6B; Gao et al., 1999; Grueber et al., 2002; Sugimura et al., 2003). In contrast, ddaE in the mutant larvae did not display such a comb-like design of dendritic arbors (Figures 6C–6F). The mutant neurons at the comparable stage had produced supernumerary terminals (Table 1) that did not necessarily show the oriented growth. About 20% of the mutant ddaE cells did not extend lateral primary branches, and in extreme cases, a single mutant ddaE extended two primary branches dorsally instead (arrowheads in Figure 6F). Similar pattern defects were also seen for the ventral class I neuron vpda (Figures 6I–6L).

Next, we examined early stages of branch formation in the wild-type and mutant embryos (Figure 7). As reported previously, each wild-type ddaE elongates a primary branch in the dorsal direction, and then secondary branches spring out and the stabilized ones tend to elongate in a straight path (arrows in Figure 7A; n = 5). In *ab* mutants, secondary branches appeared with curved morphologies and remained associated with fine higher-order branches that were frequently oriented in dorsal or ventral directions (arrows in Figure 7B; n = 10).

Postmitotic expression of *ab* cDNA in mutant ddaE and vpda rescued the abnormal pattern formation of dendrites with respect to both the directional elongation and the terminal number (Figures 6G, 6H, 6M, and 6N and Table 1). Because this GAL4 insertion did not drive transgene expression in epidermal cells or muscles that might make contact with class I dendrites, this significant rescue suggested the possibility that *ab* was necessary for proper dendritegenesis of class I neurons in a cell-autonomous fashion (see also our results of MARCM analysis next). As concerns our staining of epidermal cells and muscles and observation of larval denticles, we did not detect obvious patterning defects in those tissues in the *ab* mutants examined (data not shown).

MARCM Analysis Showed that *ab* Mutations Resulted in an Increase in the Terminal Number and the Territory Size

The above studies supported a regulatory role for Ab in controlling dendritegenesis of class I neurons. Nevertheless, the early larval lethality of the mutants limited our analysis to examine cellular phenotypes at later, third instar stages of larval development when dendritic patterns are becoming mature. We therefore generated and labeled *ab* mutant neurons in otherwise heterozygous mature larvae with the mosaic analysis with a repressible cell marker (MARCM; Lee and Luo, 1999). Dendritic arbors of both ddaD and ddaE (class I neurons) in *ab*⁻
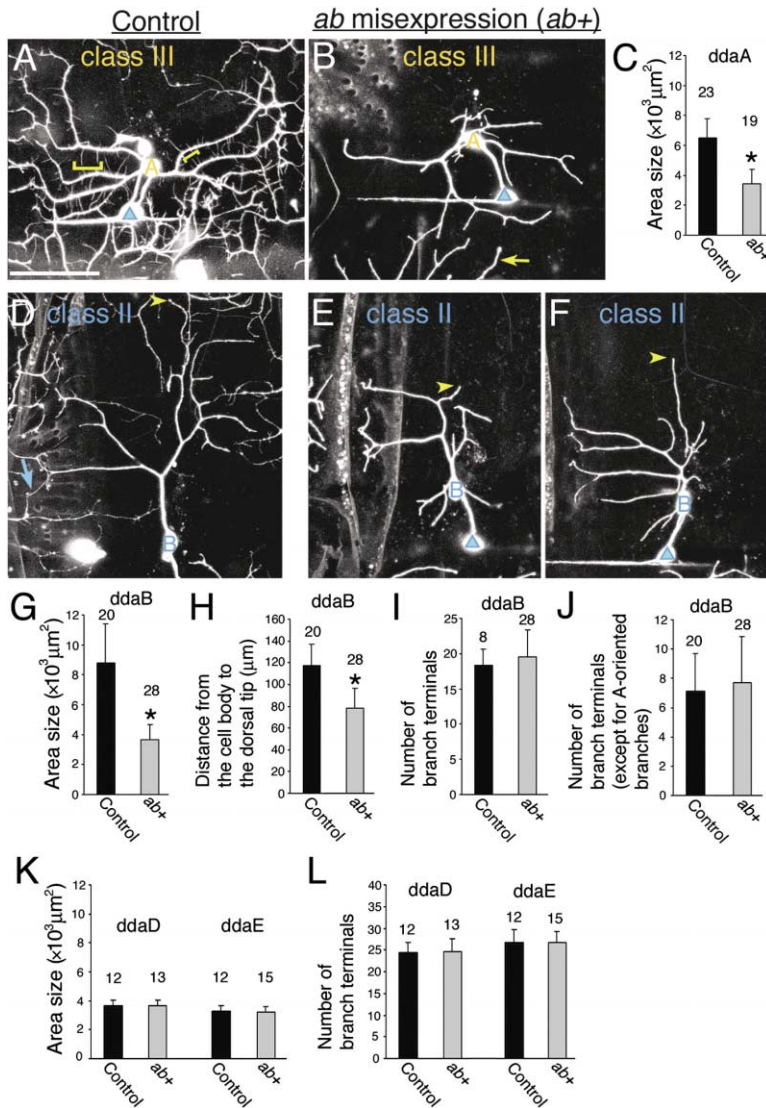
Figure 5. Effects of *ab* Transgene Expression on Dendrite Morphology of Class III ddaA, Class II ddaB, and Class I ddaD and ddaE

Single-cell analysis of a class III ddaA (A–C), a class II ddaB (D–J), and class I ddaD and ddaE (K and L).

(A, B, D–F) Morphologies of control ddaA (A) and ddaB (D) or *ab*-misexpressing ddaA (B) and ddaB (E and F). All the dorsal da neurons, except for the cells of interest, were ablated at 24–26 hr AEL; the remaining cells were imaged at around 50 hr AEL.

(A and B) Short protrusions or "spikes," which are characteristics of class III (brackets in [A]), were not formed in the *ab*-misexpressing ddaA (B). Yellow arrow indicates sparse and shorter dendritic branches that elongated from the lateral cluster.

(D–F) The *ab*-misexpressing ddaB formed a smaller dendritic field than the control cell. Arrowheads indicate the most distal tips of the dorsal branches (see H). Blue arrow in (D) points an overlap of a branch of the ddaB and that from the anterior hemisegment. Scale bar equals 50 μm for (A), (B), and (D)–(F).

(C and G–L) Quantitative analysis of control neurons and *ab*-misexpressing homologous cells. Numbers of neurons analyzed are indicated above individual bars.

(C, G, and K) Area size for ddaA (C), ddaB (G), and ddaD and ddaE (K).

(H) Distance from the most distal tip of dorsal branches to the center of the ddaB cell body. As for ddaB, a value of the size ratio of (*ab*-misexpressing cell)/(control cell) was 0.42 and that of the distance ratio was 0.66.

(I, J, and L) Number of branch terminals for ddaB (I and J) and for ddaD and ddaE (L). The number of all branches (I) and that of a subset (J) of ddaB were counted (see details in the text). Asterisks in (C), (G), and (H) represent $p < 0.001$ (Wilcoxon two-sample test). Genotypes were as described in the legend of Figure 2.

clones took on abnormal shape and produced branch terminals in excess (Figures 8A–8H) as shown in *ab* mutant young larvae. This result is consistent with the notion that the phenotypes of class I neurons in the young mutant larvae were not secondary consequences of defective epidermal or muscle development.

Under the standard protocol of MARCM analysis, embryos were collected within a short time window and developed for a fixed duration; still third instar larvae grew to different body size when clones were found and imaged. To assess whether loss of *ab* function affected the territory size of dendritic arbors in these samples, we normalized the arbor size to the size of the segment where each clone was generated (Figures 8C and 8F, see details in the legend). We found a statistically significant increase in the area size of the *ab* mutant ddaD (p < 0.01, Wilcoxon two-sample test), but not in that of the *ab* mutant ddaE.

da neurons of class II to IV did not express Ab at a detectable level, and we did not find obvious pattern defects of dendritic arbors of class II (n = 8), class III (n = 13), and class IV (n = 14, Figures 8I and 8J). The

lack of apparent abnormal phenotypes in these classes was consistent with the selective *ab* expression and its role in dendritic morphogenesis of class I neurons.

Neither *ab* Loss of Function nor Its Misexpression Was Associated with Alteration of *cut* Expression Pattern

It was earlier shown that Cut, a homeodomain protein, is expressed differentially among the four classes of da neurons and that those different expression levels control both the field size and the branching complexity of individual classes (Grueber et al., 2003a). The level of Cut is the strongest in class III, moderate in class II and class IV, and below the limit of detection in class I, which provides a contrast to that of Ab. Besides the expression profiles in da neuron classes, activities of these two genes are approximately complementary to each other with respect to gain-of-function and loss-of-function phenotypes of dendritic patterns (described below). Therefore, we explored the possibility that *ab* loss of function or its misexpression might alter the Cut expression pattern.
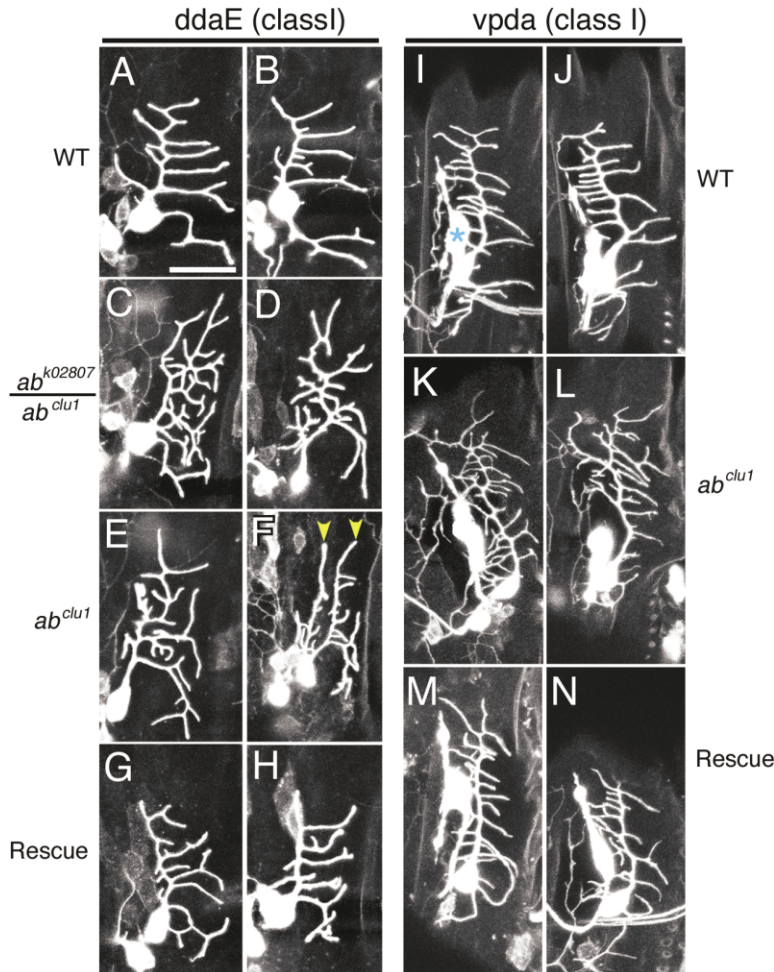
Figure 6. *ab* Loss-of-Function Altered Dendrite Morphologies of Class I Neurons ddaE and vpda

Images of two class I neurons: ddaE (A–H) and vpda (I–N) at 24–26 hr AEL.
(A, B, I, and J) wild-type (*IG1-1/mCD8::GFP*).
(C–F, K, and L) *ab* mutants. Genotypes were *IG1-1 ab^{clu1}/mCD8::GFP ab^{k02807}* (C and D) and *IG1-1 ab^{clu1}/mCD8::GFP ab^{clu1}* (E, F, K, and L).
(F) Arrowheads point to two dorsally oriented primary branches.
(G, H, M, and N) *ab* mutants, in which the *ab* transgene was expressed in ddaE and vpda, restored the normal dendritic morphologies. Genotypes were *IG1-1 ab^{clu1}/mCD8::GFP ab^{clu1}; UAS-ab-L/+* (G), *IG1-1 ab^{clu1}/mCD8::GFP ab^{k02807}; UAS-ab-S/+* (H), and *IG1-1 ab^{clu1}/mCD8::GFP ab^{k02807}; UAS-ab-L/+* (M and N).
(I) Blue asterisk denotes one of ventral chordotonal neurons.
Scale bar equals 20 μm.

Loss of *ab* function altered class I dendritic appearance toward a more branched morphology as was shown above in Figures 6–8, which is reminiscent of the altered design of class I dendritic trees upon *cut* misexpression (Grueber et al., 2003a). Thus, we examined whether Cut might be ectopically expressed in class I neurons in *ab* mutants or not; however, in all of 62 mutant hemisegments examined, Cut immunoreactivity was hardly detectable in class I neurons as in the wild-type ones (arrows in Figures 9A–9F). Conversely, *ab* misexpression reduced both the field size and the terminal number of class III and IV dendritic arbors and downsized class II arbors (Figures 3–5), which is reminiscent of loss of *cut* function phenotypes (Grueber et al., 2003a). Thus, we examined whether the *ab* ectopic ex-

pression might be associated with a dramatic decrease of the Cut level in class II-IV cells but found no such signs in any of 54 hemisegments examined (brackets and arrowheads in Figures 9G–9L).

Furthermore, we addressed whether loss of *cut* function or its ectopic expression would alter Ab expression patterns. Loss of *cut* function was not associated with the obvious appearance of Ab immunoreactivity in class II-IV neurons (Figures 9M–9R); on the other hand, *cut* misexpression reduced the level of Ab staining in class I neurons (Figures 9S–9X). When compared with the Ab immunoreactivity of epidermal cells on the same confocal section, weaker labeling was seen in dorsal class I neurons (ddaD and ddaE) (arrows in Figure 9W) but not in the ventral class I neuron (vpda). Altogether,

Table 1. Quantification of the Number of Branch Terminals for ddaE at 24–26 hr AEL		
IG1-1/mCD8::GFP	20.3 ± 2.9	(n = 108)[a]
IG1-1 ab^{clu1}/mCD8::GFP ab^{k02807}	31.0 ± 4.8	(n = 102)[a', b]
IG1-1 ab^{clu1}/mCD8::GFP ab^{clu1}	30.4 ± 4.9	(n = 100)[a'', c]
IG1-1 ab^{clu1}/mCD8::GFP ab^{k02807}; UAS-ab-S/+	22.6 ± 3.5	(n = 100)[b']
IG1-1 ab^{clu1}/mCD8::GFP ab^{k02807}; UAS-ab-L/+	23.0 ± 3.7	(n = 100)[b'']
IG1-1 ab^{clu1}/mCD8::GFP ab^{clu1}; UAS-ab-L/+	23.9 ± 3.7	(n = 108)[c']

Differences in values of the following pairs of genotypes are statistically significant (p < 0.001) according to the t test (Welch method): a-a', a-a'', b-b', b-b'', and c-c'. n: the number of ddaE examined.
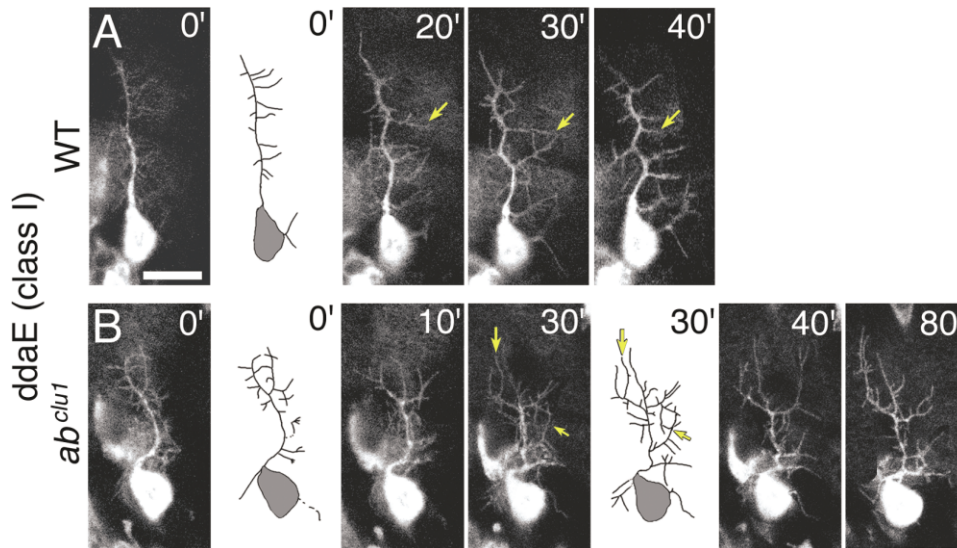
Figure 7. Time-Lapse Recordings of Class I Neuron ddaE

Time-lapse recordings of ddaE in embryos homozygous for *IG1-1 mCD8::GFP* (A) and for *IG1-1 mCD8::GFP ab^clu1^* (B).

(A) In the control embryo, secondary branches sprang out from the lateral side of the existing primary branches, extended straight, and exhibited cycles of extension and retraction (arrows).

(B) In the *ab^clu1^* embryo, secondary branches showed curved growth (arrows) and some of them extended long either dorsally or ventrally. Scale bar equals 10 μm.

our analysis did not provide strong evidence for interactions between *ab* and *cut* at the level of regulation of gene expression.

cut Overexpression Interfered with the Effect of *ab* Misexpression and Vice Versa

We next addressed whether *ab* and *cut* could interfere with each other's function at the level of dendritic morphology (Figure 10). *ab* misexpression reduced both the field size and the terminal number of class III neurons that normally express Cut at the highest level among da classes, as described above (Figures 5A–5C), and this *ab*+ phenotype became less severe when *cut* was co-overexpressed (Figures 10A and 10B). One easy landmark was spike formation; *ab* misexpression resulted in almost complete loss of spikes, which was partially recovered by co-expressing *cut* (see bracket in Figure 10B). The suppression effect of *cut* overexpression was shown to be statistically significant in terms of both the number of branch terminals and the area size (Figures 10C and 10D; p < 0.01, Wilcoxon two-sample test).

We then found that *ab* and *cut* interacted with each other in the reverse direction as well (Figures 10E–10I). *cut* misexpression in class I cells, which normally expressed *ab*, induced dendritic overgrowth and overbranching, and some of short branches were reminiscent of spikes as previously reported (compare Figures 10E and 10F and see bracket in 10F; Grueber et al., 2003a). These effects of *cut* misexpression were partially suppressed by coexpressing *ab* (Figures 10G–10I). This suppression by the coexpression of *cut* and *ab* might be due to a decrease in the level of misexpressed Cut by increasing the number of UAS transgenes to which GAL4 binds if the number of GAL4 molecules is limited.

This appeared to be unlikely, because in contrast to the full-length Ab protein, expression of a truncated form Ab-SN did not show such an interference activity (data not shown; see also Supplemental Figure S1 at http://www.neuron.org/cgi/content/full/43/6/809/DC1). All these results supported mutual interference between Ab and Cut in dendrite pattern formation under the overexpression condition.

Discussion

On the basis of previous descriptive studies on cellular behaviors of individual classes of da neuron (Grueber et al., 2002, 2003b; Sugimura et al., 2003), we addressed molecular mechanisms underlying the distinctive modes of dendrite development. Both our misexpression and loss-of-function analyses supported the hypothesis that selective expression of *ab* in class I da neurons plays a pivotal role in forming dendritic arbors, which are characteristic of the class I cells, and that development of more complex arbors of class II-IV neurons depends on the absence of Ab. We drew this conclusion not only from quantification of the number of terminals and the area size of individual dendritic trees at single given developmental stages, but also from time-lapse recordings to monitor dynamic behaviors at embryonic and/or larval stages.

As far as our analysis with molecular markers was concerned, neither *ab* misexpression nor its loss of function resulted in alteration of cell identity of da classes examined. The molecular tools employed were enhancer-trap markers for class I (ddaE) or class IV and the level of Cut that distinguishes between class I and II-IV (Grueber et al., 2003a). Thus, it appears unlikely that the dendritic phenotypes reported could be indirect
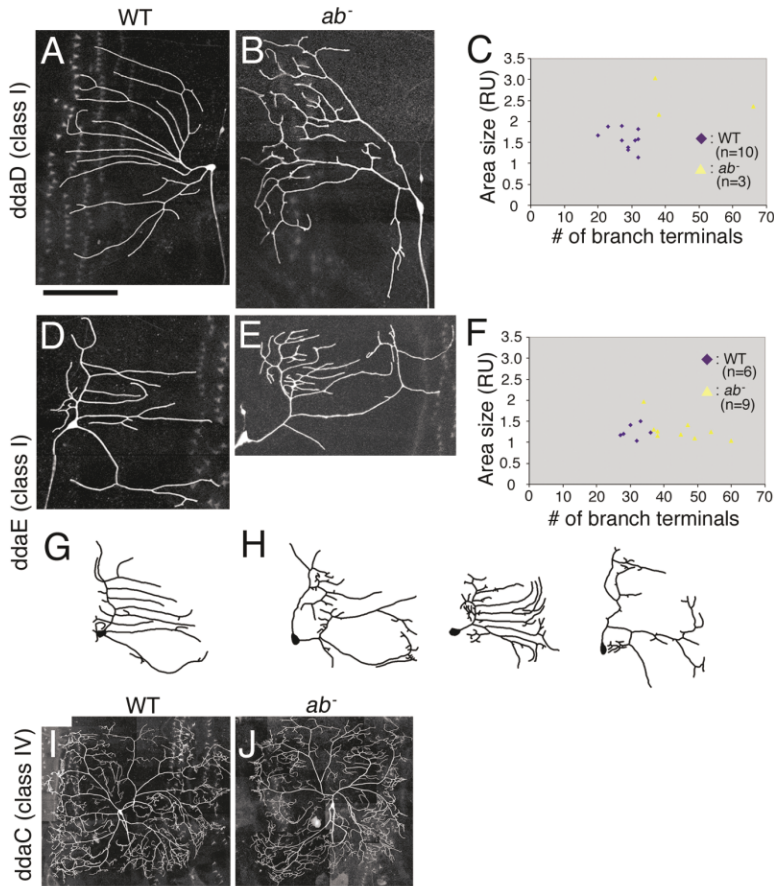
Figure 8. MARCM Analysis of *ab* Mutant Clones

(A, B, D, E, G–J) MARCM clones of ddaD (A and B), ddaE (D, E, G, and H), and ddaC (I and J). Wild-type clones (A, D, G, and I), *ab*[k02807] clones (B, E, and H), and *ab*[clu1] clone (J). (B and E) *ab*[k02807] class I clones formed deformed comb-like arbors that should have consisted of laterally oriented secondary branches.

(C and F) Numbers of branch terminals and normalized territory size of individual arbors were plotted. Blue diamonds represent wt clones; yellow triangles indicate *ab* mutant clones. To normalize the arbor size in larvae of different body size, the size of each polygon connecting dendritic tips was divided by the square of the distance between the cell body and the landmark denticle (relative unit, RU). The increase in both the terminal number and the arbor size was statistically significant for ddaD and increase in the terminal number, for ddaE ($p < 0.01$, Wilcoxon two-sample test).

(G and H) Tracings of wild-type ddaE clone (G) and *ab*[k02807] clones (H) that were normalized in terms of body size. Bars, 100 μm for (A), (B), (D), (E), (I), and (J).

consequences of cell identity alteration; we would prefer an alternative hypothesis that Ab is more immediately involved in regulating dendritic morphology through transcriptional regulation of its target genes.

ab misexpression decreased the number of branch terminals of class III and IV neurons, and conversely, *ab* mutant class I cells produced supernumerary branches. One possible interpretation of these results would be that Ab may negatively regulate dendritic branching in a broad range of neuronal types. However, this hypothesis would be difficult to reconcile with our following findings: in normal development, the territory size of class I dendrites is smaller than that of class II ones, while the dendritic trees of both classes are similarly complicated (Grueber et al., 2002). *ab* misexpression in class II neurons reduced the territory size, but the terminal number did not change significantly. Furthermore, *ab* misexpression in any da neuron of class II-IV in the dorsal cluster reduced the size and/or the terminal number to values that were comparable to those of class I neurons of the same cluster. The easiest interpretation of these results would be that the misexpression morphologically altered class II-IV dendrites toward that of class I. It should be also noted that dendritic patterns are defined not only by the numerical parameters such as the terminal number or the territory size, but also by other properties such as the comb-like design of class I, spike protrusion of class III, and mutual avoidance of class IV. Effects of *ab* loss of function or misexpression were consistent

with the notion that Ab endows every feature of class I dendritic patterning.

Although our manipulations of *ab* misexpression caused severe and reproducible phenotypes, they did not necessarily provide evidence for almost complete morphological transformation from classes II-IV into class I neurons. Class II, III, or IV neurons that had misexpressed *ab* was morphologically recognized as such, in terms of the number and the direction of dendritic shafts that grew out of each cell body and the branching pattern within the region proximal to the soma. Previous time-lapse recordings showed that da neurons of class I and class IV use distinct strategies from the very beginning of dendritic birth from the soma that contribute to differences in their basic arbor patterns (Sugimura et al., 2003). The partial alteration of the arbor patterns by *ab* misexpression might be due to a late onset and/or a low level of *ab* transgene expression obtained by using the available postmitotic drivers.

In contrast to the formation of supernumerary branch terminals of class I neurons in the *ab* mutants, the same cells did not show obvious expansion of the arbor size compared with the control cells; this could be due to the possibility that the expansion, if any, was too small to be detected at the early larval stage when differences in the field size of class I and that of other classes were subtle compared with those at late larval stages. We performed MARCM analysis to explore phenotypes at late larval stages and showed that ddaD increased in
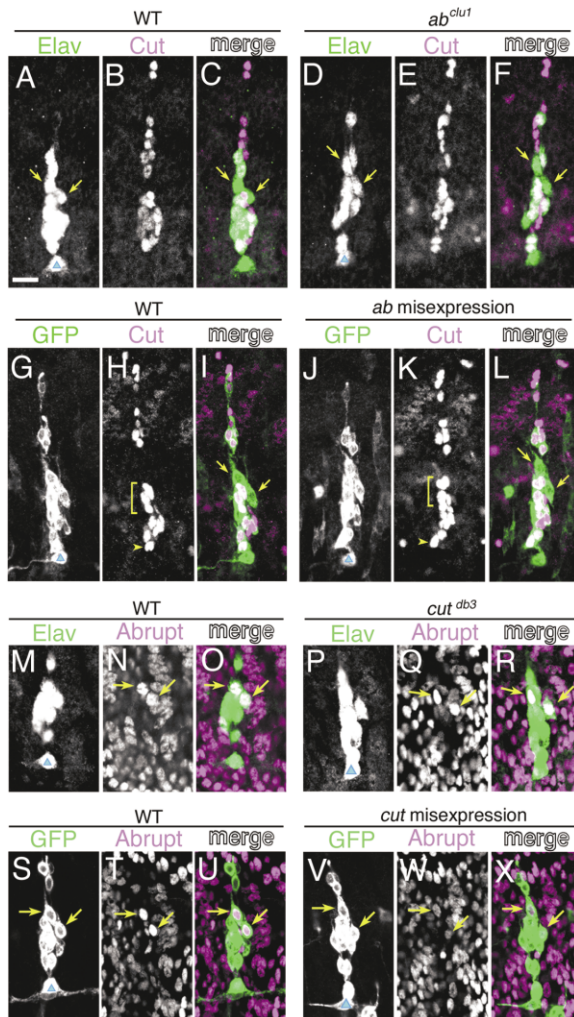
Figure 9. *ab* Mutations or *ab* Ectopic Expression Did Not Alter Cut Expression Pattern

(A–F) The wild-type (A–C) and *ab^clu1* homozygous embryos (D–F) were stained for a panneuronal marker Elav (A and D, green in C and F) and for Cut (B and E, magenta in C and F). In the *ab* mutant, Cut immunoreactivity was hardly detected in class I neurons as in the wild-type (arrows in A, C, D and F). The same result was obtained for *ab^k02807* homozygotes (data not shown).

(G–L) Control embryo (*elav-GAL4 UAS-mCD8::GFP/+* or *Y*; [G]–[I]) and the one that misexpressed *ab* in all neurons (*elav-GAL4 UAS-mCD8::GFP/+* or *Y*; *UAS-ab-L/+*; [J]–[L]) were stained for GFP (G and J, green in I and L) and for Cut (H and K, magenta in I and L). *ab* misexpression did not result in a dramatic decrease in the level of Cut staining or obvious alteration of the number of Cut-positive cells in the cluster. Compared with the pan-da drivers that were used in ectopic expression in Figures 2–5, *elav-GAL4*, which was used in this experiment, initiates transgene expression earlier in postmitotic neurons. Embryos of *elav-GAL4 UAS-mCD8::GFP/+* or *Y*; *UAS-ab-L/+* did not hatch, so they could not be used for analysis of larval dendritic development.

(M–R) The wild-type (M–O) and *ct^db3* hemizygous embryos (P–R) were stained for Elav (M and P, green in O and R) and Ab (N and Q, magenta in O and R). No other neurons were labeled as brightly as class I neurons in the wild-type and in the *ct* mutant (arrows). The same result was obtained for *ct^c145* hemizygotes (data not shown).

(S–X) Control embryo (S–U) and one that misexpressed *ct* in all neurons (V–X) were stained for GFP (S and V, green in U and X) and for Ab (T and W, magenta in U and X). Genotypes were *elav-GAL4 UAS-mCD8::GFP/+* or *Y* (S–U) and *elav-GAL4 UAS-mCD8::GFP/+* or *Y*; *UAS- cut^5/+* (V–X). Nuclei of class I neurons are indicated with arrows. (W) Two dorsal class I neurons showed a decrease in the level of Ab immunoreactivity when compared with that of epidermal cells in the same confocal image.

Throughout this figure, images of every pair of the control and the mutant or the *ab* misexpressing embryo were acquired and processed with identical parameters. Scale bar equals 10 μm.

its arbor size, but that another class I neuron examined, ddaE, did not. This variation could be explained by perdurance of the wild-type protein in each mutant cell (Lee and Luo, 1999). Alternatively, dysfunction of Ab-dependent mechanisms might not have been sufficient for expansion of the territorial field, and an additional mechanism, which works in classes II-IV neurons in normal development, may be required.

The Ab protein has two zinc fingers of the C_2H_2 class, which is one of the most common types of DNA binding domains; in addition, a BTB/POZ domain is found at the N terminus of the fingers (Hu et al., 1995). The BTB/POZ domain is an evolutionarily conserved protein-protein interaction domain, and BTB/POZ domains of several zinc finger proteins, such as PLZF and Tramtrack, have been shown to be responsible for transcriptional regulation (Zollman et al., 1994; Wong and Privalsky, 1998). Recent studies have discovered several putative transcriptional factors of other families that regulate morphological heterogeneity of dendrites including branching complexity, field size, and targeting specificity in different model systems, suggesting that transcriptional regulation is a common mechanism to generate morphological diversity of dendrites (Moore et al., 2002; Grueber et al., 2003a; Komiyama et al., 2003; Grueber and Jan, 2004). Therefore, it is likely that class-specific profiles of gene expression controlled by these factors are responsible for distinctive dendritic morphogenesis. Target genes of these transcriptional regulators in the context of dendritic pattern formation have not yet been found, and their future identification should give us detailed pictures of the molecular machineries at work.

Ab and Cut provided striking contrasts to each other in terms of class-dependent levels of immunoreactivity and, furthermore, gain-of-function and loss-of-function phenotypes of dendritic morphology (Grueber et al., 2003a, and this study). We found that neither *ab* loss of function nor its misexpression was associated with alteration of *cut* expression, which did not provide evidence for a simple epistatic or mutually dependent relationship between the two genes at the level of gene expression. It could be that selective expression of Ab and that of Cut are operated by a mechanism that is separate, at least partially. When the two putative transcription factors were examined at the level of dendritic morphology as a final read-out, we found that they could interfere with each other's function upon overexpression, which argues against a simple epistatic relationship between them. A couple of possibilities could explain this mutual interaction. For example, target genes of Ab and those of Cut may be partially overlapped, and the interference may be due to competitions between the two for *cis* regulatory elements of the same target gene. Alternatively, Ab's targets and those of Cut may operate on cytoskeletal reorganization in different ways.
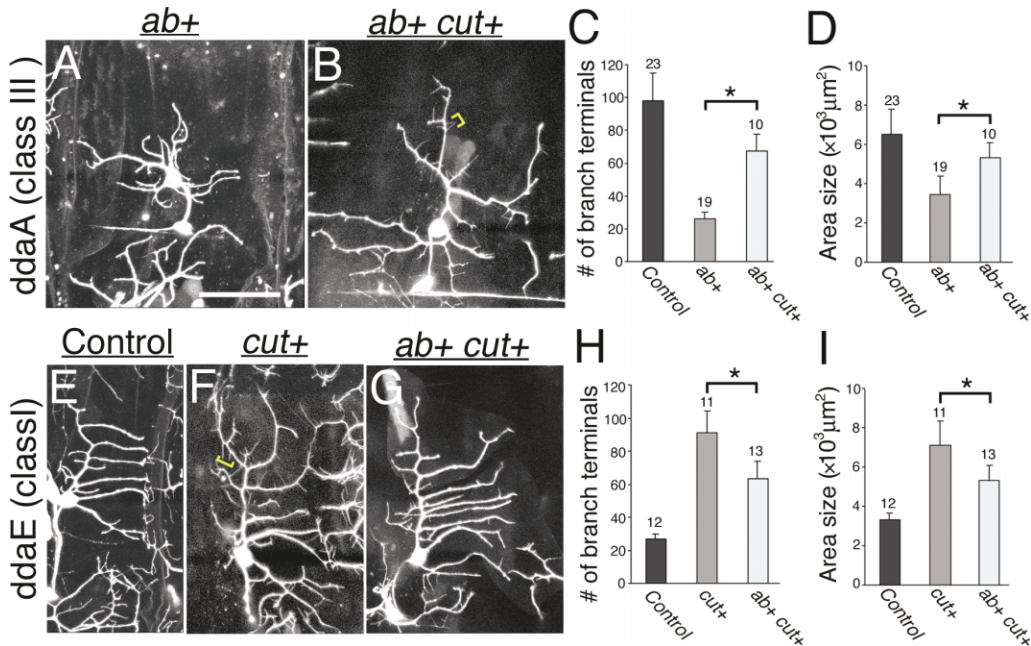
Figure 10. *cut* Overexpression Interfered with the Effect of *ab* Misexpression, whereas *ab* Overexpression Interfered with the Effect of *cut* Misexpression

Single-cell analysis of a class III ddaA (A–D) and a class I ddaE (E–I) was done as in Figure 5.

(A and B) *ab*-misexpressing ddaA hardly produced spike-like protrusions (*ab*+, [A]); in contrast, ddaA that overexpressed both *ab* and *cut* (*ab*+ *cut*+, [B]) did (for example, see bracket in [B]).

(E–G) Control ddaE (E), *cut*-misexpressing ddaE (*cut*+, [F]), and ddaE that overexpressed both *ab* and *cut* (*ab*+ *cut*+, [G]). *cut*+ ddaE made spike-like protrusions (bracket in [F]), whereas its number per cell was greatly reduced in *ab*+ *cut*+ ddaE (G).

(C, D, H, and I) Quantitative analysis of the number of branch terminals and the area size for ddaA (C and D, respectively) and for ddaE (H and I, respectively). Numbers of neurons analyzed are indicated above individual bars. Asterisks represent p < 0.01 (Wilcoxon two-sample test). Genotypes of the control and *ab*+ larvae were as described in the legend of Figure 2. Those of the *cut*+ and *ab*+ *cut*+ larvae were *IG1-2 109(2)80 GFP[S65T]/UAS-cut[5]* and *IG1-2 109(2)80 GFP[S65T]/UAS-cut[5]; UAS-ab-S/+*, respectively.

Scale bar equals 50 μm for (A), (B), and (E)–(G).

Molecular basis of the mutual interaction between Ab and Cut should be clarified by identifying their target genes.

Recent functional studies support the involvement of da neurons in thermo- and/or pain sensation and in coordination of rhythmic locomotion (Ainsley et al., 2003; Liu et al., 2003; Tracey et al., 2003). Interesting questions include whether distinct classes of da neurons or, more specifically, distinct class-specific morphological features of dendritic arbors, are responsible for distinctive physiological roles or not. This question might be addressed by monitoring the behavior of animals, in which all da neurons have class I-like dendritic patterns. Combinations of genetic and physiological approaches in this model system may shed light on a longstanding question of how each dendritic form relates to its function at the various levels, molecular, cellular, and whole body.

Experimental Procedures

Molecular Cloning

Among known splice variants of *abrupt* (*ab*), two of them produced partially distinct proteins. One of them encodes a previously reported protein (904 amino acids in length; Hu et al., 1995), and it was designated as Ab-L in this manuscript. Another encodes Ab-S, which lacks an internal small portion of 10 amino acid residues (356–367) of Ab-L. An Ab-S-encoding cDNA, RE25924, was pur-

chased from Invitrogen. For expression in *Drosophila*, cDNA clones for Ab-L and Ab-S were inserted into pUAST (Brand and Perrimon, 1993). The NBab7-1 *ab-L* cDNA clone (S. Hu and S.C., unpublished data) was originally cloned into pNB40. The p[*UAS-ab-L*] plasmid contained the entire coding sequence flanked by 164 bp of 5′-UTR and 213 bp of 3′-UTR. The coding sequence of Ab-S was amplified using a pair of primers that had XhoI or XbaI recognition sequences and cloned into XhoI-XbaI-cut pUAST.

An insertion site of pGawB carrying *GAL4* gene (Brand and Perrimon, 1993) was determined by following the protocol of the inverse PCR method (Hayashi et al., 2002). In the genome of *NP2225*, pGawB was inserted at the nucleotide 153,801 of genomic DNA AE003631, which is equivalent to 463 nucleotides downstream of the most 5′ end of RE25924 and to ~21 kb upstream of the first codon.

***Drosophila* Strains**

To visualize dendrites of da neurons, we used the following GAL4 strains: *IG1-1*, *IG1-2*, *NP2225*, *NP7028* (Sugimura et al., 2003), *NP1161* (provided by M. Yamamoto), and *109(2)80* (Gao et al., 1999). "NP" stands for strains that were established by the NP consortium (Hayashi et al., 2002). Insertions of p[*UAS- mCD8::GFP*] and p[*UAS-GFP(S65T)*] were labeled as *mCD8::GFP* and *GFP[S65T]*, respectively. Dendrites of class I neurons were observed in *IG1-1/mCD8::GFP*, *IG1-1 mCD8::GFP*, *NP2225/mCD8::GFP*, or *NP2225 GFP[S65T]/+*; and those of class IV neurons, in *NP7028 mCD8::GFP/mCD8::GFP* or *NP1161 GFP[S65T]/NP1161*. To drive *ab* expression at a high level in all da neurons, we used a chromosome that has two GAL4 insertions (*IG1-2* and *109(2)80*). Compared to *elav-GAL4* that initiates transgene expression at an early postmitotic phase (stage 13 or earlier stages), all of our GAL4 stocks above started driving tarnsgene expression at stage 15 or later stages.

ab^{clu1} is a nonsense mutation that terminates the polypeptide at residue 531 of Ab-L (Vactor et al., 1993; Hu et al., 1995; Supplemental Figure S1 at http://www.neuron.org/cgi/content/full/43/6/809/DC1). *ab^{k02807}* is a P insertion allele (Johannes and Preiss, 2002). Each of the *ab* alleles was recombined with FRT40A for MARCM analysis, and we mated the following pairs: females of *elav-GAL4 UAS-mCD8::GFP hsFLP; tub-Gal80 FRT40A* to males of *FRT40A/FRT40A* to generate control *ab^+* clones and to males of *ab FRT40A/CyO* to generate *ab* mutant clones. To image clones, we mounted each larva in 90% glycerol in PBS on a slide between spacers made of vinyl tapes. Other strains used were null mutants of *cut* (*ct^{db3}* and *ct^{c145}*; Blochlinger et al., 1988) and *UAS-cut^5* (Hardiman et al., 2002; remobilized by C. Micchelli). All fly embryos and larvae were grown at 25°C.

Image Collection of Dendritic Trees

Effects of *ab* overexpression on dendritic morphogenesis were visualized at the single-cell level as follows: In each experiment, a stage 17 embryo or an anesthetized larva at 24–26 hr AEL was mounted, and individual da neurons in the dorsal cluster were identified under fluorescence microscope (Olympus) on the basis of their stereotypic arrangement and the shape of cell body (see details in the legend of Figures 2E and 2F). All neurons, except for a single da neuron of interest and dorsal bipolar neuron, were ablated by using Micropoint (Photonics Instruments). We selected dorsal clusters of abdominal segments 2–6 for this experiment. Following the ablations, we kept watching the embryos, and as soon as they hatched, individual larvae were returned to yeasted apple plates with forceps, gently cleaned of oil, and allowed to develop. Those larvae were anesthetized at subsequent stages and images of their dendritic trees were collected under a confocal microscope (BioRad). Details of the above and other procedures (branch severing of da neurons and time-lapse analysis) were as described (Sugimura et al., 2003; see also Grueber et al., 2003b).

Quantification

Quantitative or semiquantitative analysis was performed essentially as previously described (Grueber et al., 2002). Each dendritic field was delineated by a polygon connecting dendritic tips, and its size was calculated by using Laser Sharpe (BioRad). Total length of dendritic branches was measured by using Axiocam ver 3.1 (Zeiss). Dendritic branches and their tips of ddaA, ddaB, and ddaC were identified by monitoring individual Z-series files when necessary, and the tip number per cell was counted (for ddaB, see details in Results). As regards control ddaA and ddaC, it was sometimes difficult to pinpoint the very ends of dendritic tips at segmental boundaries, so we measured the length of each branch between a branching point and a distal-most position that we could identify. Thus, the territory size and the number of dendritic branches were underestimated for the control cells; nevertheless, *ab* ectopic expression caused statistically significant differences (Figures 3G and 5C). Data are presented as means ± SD.

Immunochemistry

Whole-mount embryos and dissected larvae were stained according to standard protocols with the following primary antibodies: rabbit anti-Abrupt (Hu et al., 1995), mouse anti-Cut (Blochlinger et al., 1990; 2B10 from Developmental Studies Hybridoma Bank at the University of Iwoa), rat anti-Elav (7E8A10; Developmental Studies Hybridoma Bank), mouse anti-GFP (Sigma), and rabbit anti-GFP (Molecular Probes).

References

Ainsley, J.A., Pettus, J.M., Bosenko, D., Gerstein, C.E., Zinkevich, N., Anderson, M.G., Adams, C.M., Welsh, M.J., and Johnson, W.A. (2003). Enhanced locomotion caused by loss of the *Drosophila* DEG/ENaC protein Pickpocket1. Curr. Biol. *13*, 1557–1563.

Blochlinger, K., Bodmer, R., Jack, J., Jan, L.Y., and Jan, Y.N. (1988). Primary structure and expression of a product from *cut*, a locus involved in specifying sensory organ identity in *Drosophila*. Nature *333*, 629–635.

Blochlinger, K., Bodmer, R., Jan, L.Y., and Jan, Y.N. (1990). Patterns of expression of *cut*, a protein required for external sensory organ development in wild-type and cut mutant *Drosophila* embryos. Genes Dev. *4*, 1322–1331.

Bodmer, R., and Jan, Y.N. (1987). Morpohological differentiation of the embryonic peripheral neurons in *Drosophila*. Rouxs Arch. Dev. Biol. *196*, 69–77.

Brand, A.H., and Perrimon, N. (1993). Targeted gene expression as a means of altering cell fates and generating dominant phenotypes. Development *118*, 401–415.

Campos-Ortega, J.A., and Hartenstein, V. (1997). The Embryonic Development of *Drosophila melanogaster* (Berlin: Springer).

Gao, F.B., Brenman, J.E., Jan, L.Y., and Jan, Y.N. (1999). Genes regulating dendritic outgrowth, branching, and routing in *Drosophila*. Genes Dev. *13*, 2549–2561.

Gao, F.B., Kohwi, M., Brenman, J.E., Jan, L.Y., and Jan, Y.N. (2000). Control of dendritic field formation in *Drosophila*: the roles of *flamingo* and competition between homologous neurons. Neuron *28*, 91–101.

Grueber, W.B., and Jan, Y.N. (2004). Dendritic development: lessons from *Drosophila* and related branches. Curr. Opin. Neurobiol. *14*, 74–82.

Grueber, W.B., Jan, L.Y., and Jan, Y.N. (2002). Tiling of the *Drosophila* epidermis by multidendritic sensory neurons. Development *129*, 2867–2878.

Grueber, W.B., Jan, L.Y., and Jan, Y.N. (2003a). Different levels of the homeodomain protein cut regulate distinct dendrite branching patterns of *Drosophila* multidendritic neurons. Cell *112*, 805–818.

Grueber, W.B., Ye, B., Moore, A.W., Jan, L.Y., and Jan, Y.N. (2003b). Dendrites of distinct classes of *Drosophila* sensory neurons show different capacities for homotypic repulsion. Curr. Biol. *13*, 618–626.

Hardiman, K.E., Brewster, R., Khan, S.M., Deo, M., and Bodmer, R. (2002). The *bereft* gene, a potential target of the neural selector gene *cut*, contributes to bristle morphogenesis. Genetics *161*, 231–247.

Häusser, M., and Mel, B. (2003). Dendrites: bug or feature? Curr. Opin. Neurobiol. *13*, 372–383.

Hayashi, S., Ito, K., Sado, Y., Taniguchi, M., Akimoto, A., Takeuchi, H., Aigaki, T., Matsuzaki, F., Nakagoshi, H., Tanimura, T., et al. (2002). GETDB, a database compiling expression patterns and molecular locations of a collection of *gal4* enhancer traps. Genesis *34*, 58–61.

Hu, S., Fambrough, D., Atashi, J.R., Goodman, C.S., and Crews, S.T. (1995). The *Drosophila abrupt* gene encodes a BTB-zinc finger regulatory protein that controls the specificity of neuromuscular connections. Genes Dev. *9*, 2936–2948.

Jan, Y.N., and Jan, L.Y. (1993). The peripheral nervous system. In The Development of *Drosophila melanogaster*, M. Bate and A. Martinez-Arias, eds. (Cold Spring Harbor, NY: Cold Spring Harbor Laboratory Press), pp. 1207–1244.

Jan, Y.N., and Jan, L.Y. (2003). The control of dendrite development. Neuron *40*, 229–242.

Johannes, B., and Preiss, A. (2002). Wing vein formation in *Drosoph-*

ila melanogaster: *hairless* is involved in the cross-talk between Notch and EGF signaling pathways. Mech. Dev. *115*, 3–14.

Komiyama, T., Johnson, W.A., Luo, L., and Jefferis, G.S. (2003). From lineage to wiring specificity. POU domain transcription factors control precise connections of *Drosophila* olfactory projection neurons. Cell *112*, 157–167.

Lee, T., and Luo, L. (1999). Mosaic analysis with a repressible cell marker for studies of gene function in neuronal morphogenesis. Neuron *22*, 451–461.

Liu, L., Yermolaieva, O., Johnson, W.A., Abboud, F.M., and Welsh, M.J. (2003). Identification and function of thermosensory neurons in *Drosophila* larvae. Nat. Neurosci. *6*, 267–273.

Mainen, Z.F., and Sejnowski, T.J. (1996). Influence of dendritic structure on firing pattern in model neocortical neurons. Nature *382*, 363–366.

Masland, R.H. (2001). Neuronal diversity in the retina. Curr. Opin. Neurobiol. *11*, 431–436.

Moore, A.W., Jan, L.Y., and Jan, Y.N. (2002). *hamlet*, a binary genetic switch between single- and multiple-dendrite neuron morphology. Science *297*, 1355–1358.

Schaefer, A.T., Larkum, M.E., Sakmann, B., and Roth, A. (2003). Coincidence detection in pyramidal neurons is tuned by their dendritic branching pattern. J. Neurophysiol. *89*, 3143–3154.

Scott, E.K., and Luo, L. (2001). How do dendrites take their shape? Nat. Neurosci. *4*, 359–365.

Sugimura, K., Yamamoto, M., Niwa, R., Satoh, D., Goto, S., Taniguchi, M., Hayashi, S., and Uemura, T. (2003). Distinct developmental modes and lesion-induced reactions of dendrites of two classes of *Drosophila* sensory neurons. J. Neurosci. *23*, 3752–3760.

Tracey, W.D., Jr., Wilson, R.I., Laurent, G., and Benzer, S. (2003). *painless*, a *Drosophila* gene essential for nociception. Cell *113*, 261–273.

Vactor, D.V., Sink, H., Fambrough, D., Tsoo, R., and Goodman, C.S. (1993). Genes that control neuromuscular specificity in *Drosophila*. Cell *73*, 1137–1153.

Vetter, P., Roth, A., and Häusser, M. (2001). Propagation of action potentials in dendrites depends on dendritic morphology. J. Neurophysiol. *85*, 926–937.

Whitford, K.L., Dijkhuizen, P., Polleux, F., and Ghosh, A. (2002). Molecular control of cortical dendrite development. Annu. Rev. Neurosci. *25*, 127–149.

Williams, D.W., and Truman, J.W. (2004). Mechanisms of dendritic elaboration of sensory neurons in Drosophila: insights from in vivo time lapse. J. Neurosci. *24*, 1541–1550.

Wong, R.O., and Ghosh, A. (2002). Activity-dependent regulation of dendritic growth and patterning. Nat. Rev. Neurosci. *3*, 803–812.

Wong, C.W., and Privalsky, M.L. (1998). Components of the SMRT corepressor complex exhibit distinctive interactions with the POZ domain oncoproteins PLZF, PLZF-RARalpha, and BCL-6. J. Biol. Chem. *273*, 27695–27702.

Zollman, S., Godt, D., Prive, G.G., Couderc, J.L., and Laski, F.A. (1994). The BTB domain, found primarily in zinc finger proteins, defines an evolutionarily conserved family that includes several developmentally regulated genes in *Drosophila*. Proc. Natl. Acad. Sci. USA *91*, 10717–10721.